Korean J. Chem. Eng., **24**(5), 897-905 (2007)

Oxygen permeability and structural stability of $La_{0.6}Sr_{0.4}Co_{0.2}Fe_{0.8}O_{3-\delta}$ membrane

Jung Hoon Park† and Sang Do Park*

Energy Conversion Research Department, Korea Institute of Energy Research (KIER), Daejeon 305-343, Korea
*Carbon Dioxide Reduction and Sequestration R&D Center,
Korea Institute of Energy Research (KIER), Daejeon 305-343, Korea
(*Received 25 August 2006 • accepted 22 February 2007*)

Abstract−$La_{0.6}Sr_{0.4}Co_{0.2}Fe_{0.8}O_{3-\delta}$ oxides were synthesized by citrate method and hydrothermal method. The oxides prepared by citrate method are perovskite type structure, while the oxides by hydrothermal method have a small amount of secondary phase in the powder. Pyrex glass seal and Ag melting seal provided reliable gas-tight sealing of disk type dense membrane in the range of operation temperature, but commercial ceramic binder could not be removed from the support tube without damage to the tube or membrane. Though the degree of gas tightness increases in the order of glass>Ag>ceramic binder, in the case of glass seal, the undesired spreading of glass leads to an interfacial reaction between it and the membrane and reduction of effective permeation area. The oxygen flux of $La_{0.6}Sr_{0.4}Co_{0.2}Fe_{0.8}O_{3-\delta}$ membrane increases with increasing temperature and decreasing thickness, and the oxygen permeation flux through 1.0 mm membrane exposed to flowing air (P_h=0.21 atm) and helium (P_l=0.037 atm) is ca. 0.33 ml/cm^2·min at 950 °C. X-ray diffraction analysis for the membrane after permeation test over 160 h revealed that La_2O_3 and unknown compound were formed on the surface of membrane. The segregation compounds of surface elements formed on both surfaces of membrane irrespective of spreading of glass sealing material.

Key sords: Ion Transport Membrane, Sealing, Perovskite Oxides, Oxygen Separation, Membrane Stability

INTRODUCTION

The IEA World Energy Outlook (WEO) Reference Scenario projects that, based on policies in place, by 2030 CO_2 emissions will have increased by 63% from today's level, which is almost 90% higher than 1990 levels [1]. Hence, stronger actions than those currently being considered by governments must be taken to avoid substantial increases over the next few decades. In the view of technology, CO_2 emission reduction options include the switch to lower carbon fossil fuels, renewable energy source, nuclear, energy efficiency and carbon capture and storage (CCS). Until now, the best available method to remove CO_2 substantially in the atmosphere is CCS, which has the potential to reduce overall mitigation costs. Moreover, the worldwide researches especially have focused on carbon capture in CCS because the cost of separating CO_2 is over 70% of the total cost. In the current status of CCS technology, there are three different types of CO_2 capture systems: post combustion, pre-combustion and oxy-fuel combustion [2]. The oxy-fuel combustion process eliminates nitrogen from the flue gas by combusting a hydrocarbon or carbonaceous fuel in either pure oxygen or mixture of pure oxygen and a CO_2-rich recycled flue gas. Oxygen is the key requirement for any oxy-fuel combustion system. To commercialize an oxy-fuel combustion system, a more economical process than the existing method is still necessary because the bottleneck of oxy-fuel combustion is the oxygen production cost. It is also a key technology for pre-combustion CO_2 capture. Current existing methods of oxygen production by air separation comprise cryogenic distillation, adsorption using multi-bed pressure swing units and polymeric membranes. While a membrane system using ceramic mixed metal oxides has recently been developed to obtain high efficiency and low oxygen production cost in combustion temperatures above 500 °C and preferably above 700 °C. In particular, dense mixed-conducting ceramic membranes are of significant interest due to potential application for high-purity oxygen separation from air [3,4]. The main advantages of such membranes include an infinite theoretical permselectivity with respect to oxygen.

Among the oxygen ion transport membranes (ITM), perovskite-type (ABO_3) ceramic membranes exhibit the highest oxygen permeability due to their high ionic and electronic conductivity. Teraoka et al. [5-7] were the first to report high oxygen permeation flux through several $La_{1-x}Sr_xCo_{1-y}Fe_yO_{3-\delta}$ perovskite membranes. When A-site of perovskite is doped with lower valence state metal ions (such as partial substitution of La^{3+} by Sr^{2+} in $LaCoO_{3-\delta}$), oxygen vacancies as well as a change in the valence state of the B ions in the lattice will occur in order to maintain the electronic neutrality. A suitable membrane for practical applications should possess both sufficiently high oxygen permeability and sustainable structural stability. The operating temperature of these membranes is typically between 600 and 1,000 °C. Practical applications for oxy-fuel combustion or oxygen separation for pre-combustion process and experimental studies of these ceramic membranes require sealing a membrane to a dense ceramic or metal support tube. Commonly used rubber O-ring seals are not suitable for these applications due to their heat resistance limits (<400 °C). Inorganic materials with high melting points or metal sealing can be used for sealing the ceramic membranes at high temperatures (>600 °C) [8-10].

In this work, powder for ionic transport membrane has been syn-

†To whom correspondence should be addressed.
E-mail: pjhoon@kier.re.kr
‡This paper was presented at the 6th Korea-China Workshop on Clean Energy Technology held at Busan, Korea, July 4-7, 2006.

thesized and the oxygen separation experiment has been conducted to investigate the sealing effect and the oxygen permeability of ceramic type membrane. The membrane based on perovskite-type $La_{0.6}Sr_{0.4}Co_{0.2}Fe_{0.8}O_{3-\delta}$ (LSCF-6428) was chosen in this work due to its high oxygen permeation and good structure and chemical stabilities reported in our previous study [11,12]. The purpose of this study was to investigate the oxygen permeability of ceramic membrane and to characterize the structure changes of the membrane before and after oxygen permeation for inorganic sealing materials.

EXPERIMENTAL

1. Synthesis and Characterization of ITM Material

Materials of ionic transport membrane for oxygen separation have been synthesized by citric acid method and hydrothermal process and have examined whether perovskite structure formed. In citric acid method, perovskite type oxides were prepared using La, Sr, Co and Fe nitrates (>99%, Aldrich) and citric acid (98%, Junsei Co.) as starting materials. The nitrates were weighed according to the nominal composition of $La_{0.6}Sr_{0.4}Co_{0.2}Fe_{0.8}O_{3-\delta}$. The reactant was dissolved in water and reacted at 100 °C for 3-4 h and then the solution obtained was dried at 80 °C. Finally, a dark brown gel was calcined at 500-1,300 °C to prepare perovskite type oxide (CA-LSCF-6428). In the case of hydrothermal reaction, starting materials were $La(OH)_3$ (99.9%, Aldrich,), $Sr(NO_3)_2$ (99+%, Aldrich), $Co(NO_3)_2 \cdot 6H_2O$ (98+%, Aldrich), and $Fe(NO_3)_3 \cdot 9H_2O$ (98+%, Aldrich) with or without ammonia (25.0-28.0%, Dongyang Chemical) and the mixture of starting materials and water reacted at 250-450 °C to obtain the final powder (HT-LSCF-6428). The schematic diagrams of manufacturing processes are summarized in Fig. 1. The as-synthesized powders were compressed into disk membranes of 25.4 mm in diameter and 1.0-2.0 mm in thickness in a stainless steel mold under a hydraulic load of 40 ton on an area of 5.07 cm^2 by unilateral press (model 25601 series, Specac Limited, U.K.). After 10 min, the pressure was released and the die was removed from the press. The green disks were then sintered at 1,200-1,300 °C for 5-10 h, with a heating and cooling rate of 1-2 °C/min. The sintered membrane has an outer diameter of about 20.5 mm. The sintered membrane disks were polished with 600 grit SiC on both surfaces by a grinder (Beta series, Buehler LTD., U.S.A) to smooth the surface of the membrane and to control the thickness of membrane.

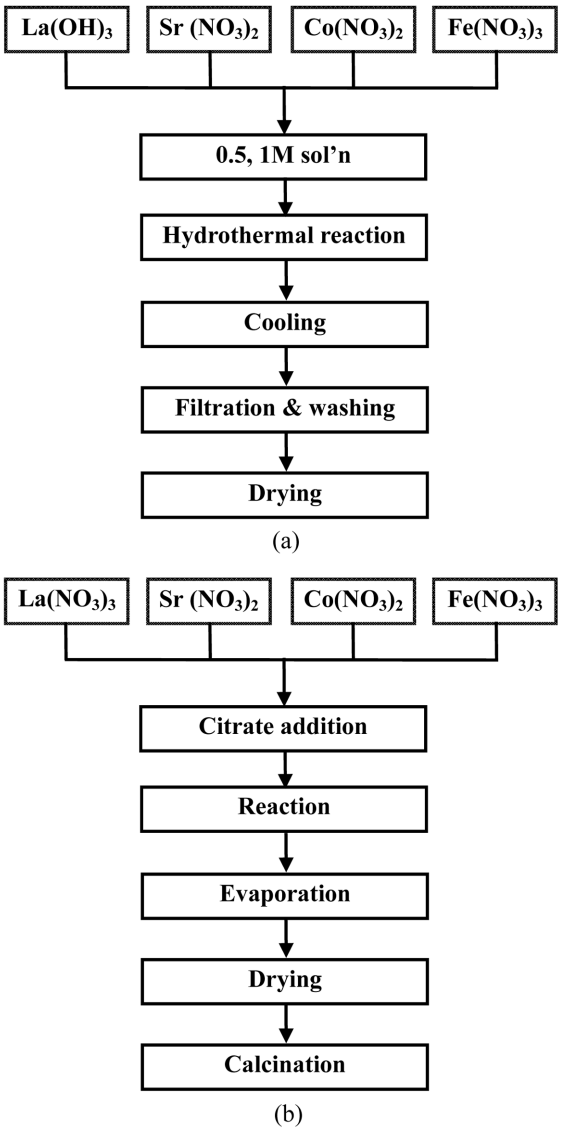

Fig. 1. Experimental procedures for synthesis of LSCF using (a) hydrothermal method and (b) citric acid method.

Thermogravimetric (TG) analysis of the gel was performed by Thermal Analyzer-SDT600 (TA instrument, U.S.A.) at a heating rate of 5 °C/min in air. The crystal structures of the powder and the sintered disk membrane before and after oxygen permeation were characterized with an X-ray diffractometer (XRD, Rigaku Co Model D/Max 2200-Ultimaplus, Japan) and a scanning electron microscope (SEM, Model 1530, LEO Co. Germany). After permeation, the surface of membrane was examined by using a stereomicroscope (SZX12, Olympus, Japan).

2. Oxygen Permeation Measurement

The membrane permeation test apparatus used in this work is shown in Fig. 2. A disk type permeation cell was used in this work for the oxygen permeation study. A ceramic glass ring, a ceramic bond (P24, Tokuriki Chemical) and Ag ring (Ag plate, 99.9%, Aldrich) were used as the sealant to seal the disk onto the dense alumina tube. The membrane permeation cell was assembled with the membrane, alumina tubes and sealants, and the temperature of the cell was increased up to 950 °C with a heating rate of 1.5 °C/min and held at this temperature for 30 min to seal the membrane disk and the alumina tube. The leakage test for the outer parts of apparatus such as line, fitting and valve was conducted with N_2 gas at 600 °C prior to oxygen permeation test. The leakage through membrane during oxygen permeation test was also measured for all runs at each temperature and the oxygen permeation fluxes were corrected on the basis of the measured leakage. A permeation experiment is considered as failure in the case of over 5% leakage. In addition, effective inner surface area and phase change of membrane disks after sealing was analyzed to investigate the effect of sealant. A permeation study was performed within the temperature range of 750-950 °C. Synthesis air (21.2 vol% O_2+78.8 vol% N_2) and pure He (99.999%) were introduced into the different side of the membrane disk and were controlled by the mass flow controller. The feed flow rate was kept at 20 ml/min, and sweep flow rate was 20 ml/min on the permeated side. The oxygen content in the permeate

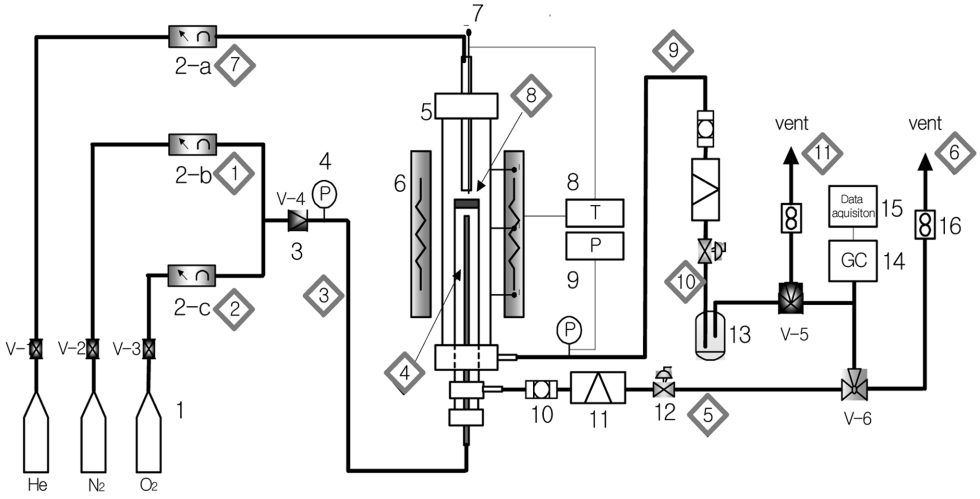

Fig. 2. Schematic diagram of experimental apparatus.

1. Gas cylinder	5. Membrane reactor	9. Pressure transducer	13. Water trap
2. Mass flow controller	6. Furnace	10. Line filter	14. Gas chromatography
3. Check valve	7. Thermocouple	11. Cooler	15. Data acquisition system
4. Pressure gauge	8. Temperature controller	12. Back pressure regulator	16. Flow meter

stream was measured with a gas chromatograph (GC-TCD, Acme 6000, YoungLin, Korea). Hydrogen was used as a reference gas, and a 1.8 m 5A molecular sieve was employed for gas separation. The gas chromatograph was frequently calibrated by using standard gases of oxygen in helium in order to ensure reliability of the experimental data. Using the results of GC, the oxygen flux was determined by

$$J_{O_2}\,[\mathrm{ml/min\cdot cm^2\ (STP)}] = \frac{F_{permeation}[\mathrm{ml/min(STP)}]\,y_{O_2}[\mathrm{v\%}] - \text{leakage correction}}{A[\mathrm{cm^2}]} \quad (1)$$

Where $F_{permeation}$ is the total flow rate of the permeation stream in which the oxygen concentration is y_{O_2}, A is the effective membrane surface area, and leakage correction is the calculating oxygen flux from leakage.

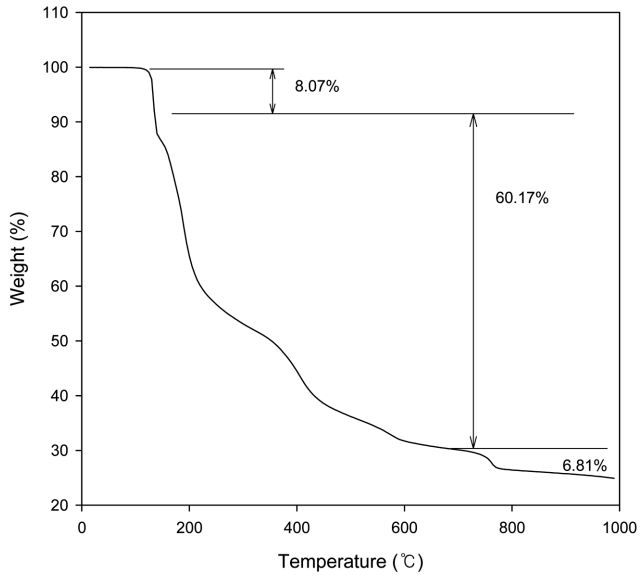

Fig. 3. TGA results of the CA-LSCF-6428 gel.

RESULTS AND DISCUSSIONS

1. Crystal Structure of Ceramic Powder

Fig. 3 shows the thermogravimetric analysis (TGA) of the LSCF

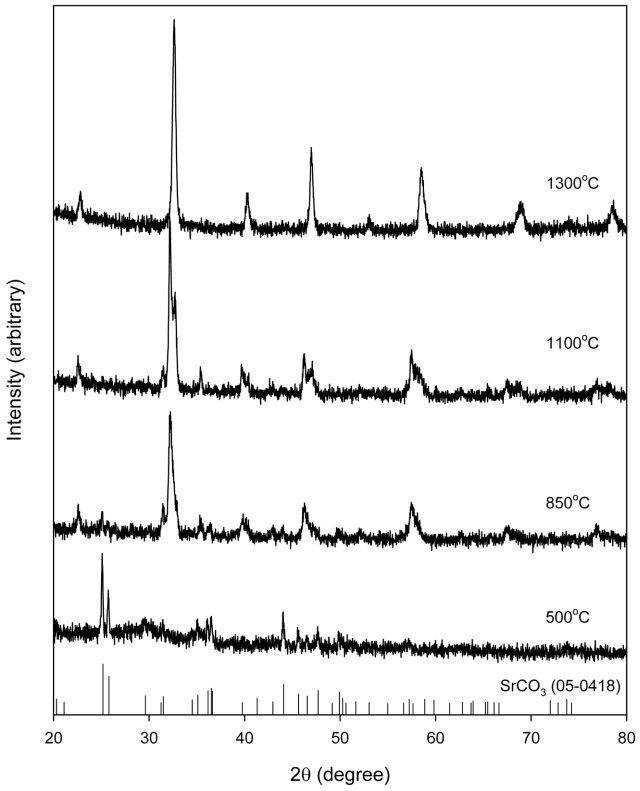

Fig. 4. XRD patterns of CA-LSCF-6428 oxides calcined at various temperatures.

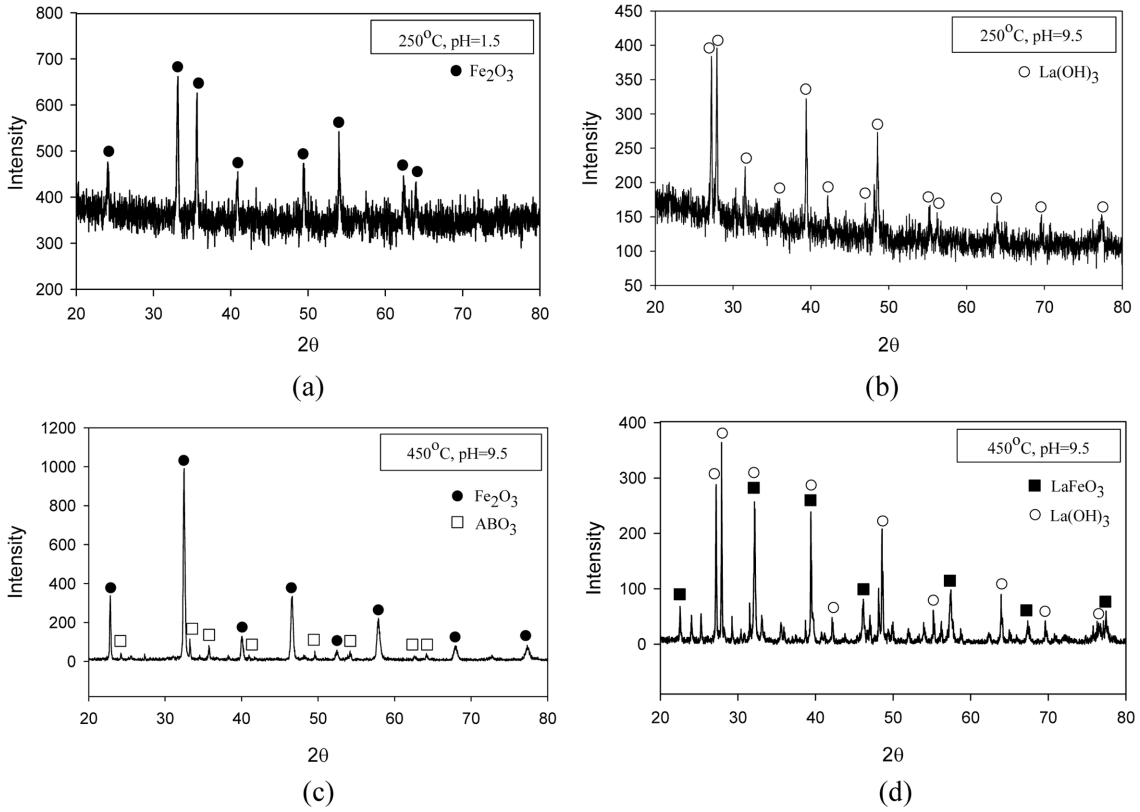

Fig. 5. XRD patterns of powders prepared under various conditions by hydrothermal method.
(a) Powder prepared with $La(OH)_3$, and $Fe(NO_3)_3 \cdot 9H_2O$ at 250 °C without ammonia water
(b) Powder prepared with $La(OH)_3$, and $Fe(NO_3)_3 \cdot 9H_2O$ at 250 °C with ammonia water
(c) Powder prepared with $La(OH)_3$, and $Fe(NO_3)_3 \cdot 9H_2O$ at 450 °C with ammonia water
(d) HT-LSCF-6428 powder prepared at 450 °C with ammonia water

gel derived from the precursor solution by citrate method. A small weight loss of 8.07% by 135 °C is ascribed to the evaporation of residual water. In the range of 150-650 °C, there are two successive weight losses, which are assigned to the decomposition and combustion of the citrate complex, respectively. This result is in good agreement with the report of Xu et al. [13]. However, no further weight loss appears over 600 °C in the results of Xu while 6.81% weight loss is seen in the TGA curve after 600 °C. Based on the XRD results, the small weight loss in the range of 700-900 °C can be attributed to decomposition of $SrCO_3$. From TGA results, the calcinations temperature is determined over 850 °C at which the weight loss is almost constant. Fig. 4 shows the comparison between X-ray diffraction patterns of the CA-LSCF-6428 calcined in the range of 500-1,300 °C and standard peak of $SrCO_3$ (JCPDS No. 05-0418). The X-ray pattern of the powder calcined at 500 °C contains only one main phase, $SrCO_3$ while the X-ray pattern of the powder calcined at 850 °C and 1,100 °C contains perovskite LSCF and a trace of $SrCO_3$. However, upon increasing the calcinations temperature to 1,300 °C, the peaks of $SrCO_3$ almost disappear due to the decomposition of $SrCO_3$, and the perovskite phase is developed. These results are different from the X-ray results of Xu et al. and Jin et al. [14]. The peaks of $SrCO_3$ in their results disappeared at temperature less than 800 °C. In our work, only citric acid was used as chelating agent, while Xu et al. added ethylene glycol and nitric acid to citrate salts and Jin et al., ammonia solution. Namely, different start materials seem to cause the different results of TGA and XRD. An interesting observation is that the pH of solution is key factor to control the impurity such as $SrCO_3$ at lower calcination temperature.

In contrast to the citrate method, XRD pattern of the powder (HT-LSCF-6428) prepared by hydrothermal process revealed that the powder consists of a mixture of $LaFeO_3$ and Fe_2O_3. To investigate the main parameters governing in the hydrothermal reaction, 2-component powders were prepared with $La(OH)_3$, and $Fe(NO_3)_3 \cdot 9H_2O$ by hydrothermal method without or with ammonia addition ((a)-(c) in Fig. 5). Fig. 5 shows XRD results of powders prepared with 2-components according to various conditions and XRD pattern of powder prepared with $La(OH)_3$, $Sr(NO_3)_2$, $Co(NO_3)_2 \cdot 6H_2O$, and $Fe(NO_3)_3 \cdot 9H_2O$ as to the molar ratio of La : Sr : Co : Fe=0.6 : 0.4 : 0.2 : 0.8 by hydrothermal method with ammonia water at 450 °C. In the region of lower pH, i.e., (a) in Fig. 5, Fe_2O_3 is stable and no lanthanum ferrite is formed at this condition. While, in the higher pH ((b) and (c) in Fig. 5), it is known that $La(OH)_3$ and $LaFeO_3$ are stable at the condition of 250 °C and 450 °C with ammonia. On the contrary of 2-component reaction, perovskite structure is formed as main product in the case of 4-component reaction, i.e., (d) in Fig. 5. The contents of Fe_2O_3 also decrease considerably. It is notable that the effect of pH in solution is more dominant than that of temperature and pressure when perovskite type oxides were prepared by hydrothermal method.

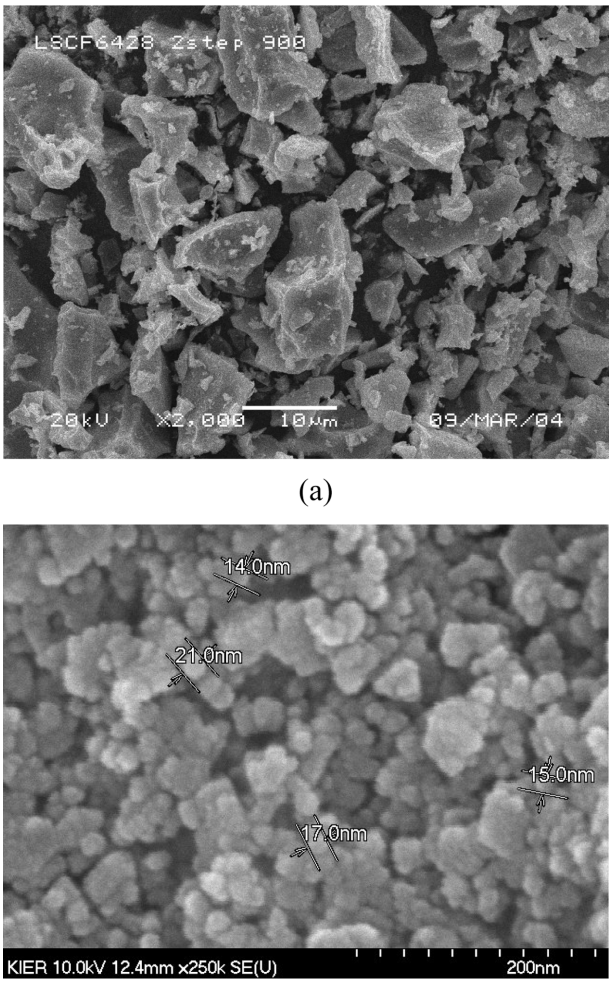

Fig. 6. SEM images of a LSCF-6428 ceramic powders prepared by (a) citrate method and (b) hydrothermal method.

Fig. 6 presents the SEM images of oxides (CA-LSCF-6428 and HT-LSCF-6428) prepared by citrate method and hydrothermal method, respectively. As shown in Fig. 6(a), the powder morphology of CA-LSCF-6428 oxides is considerably coarse and the particle size distribution is also broad in the range of about 1-10 μm. It indicates that this citrate method is close to the solid state reaction because the organic acid is burnt over 600 °C. On the other hand, SEM observations of HT-LSCF-6428 revealed a relatively homogeneous size distribution of nano-sized spherical particles. When particle size is small and homogenous, the sintering temperature can decrease, resulting in dense membrane at low sintering temperature. If single phase perovskite type oxide is obtained by hydrothermal reaction, it can be more positive over other preparation methods such as solid state reaction and citrate method.

2. Leakage Test of Sealing Material

The most common method to seal a dense ceramic membrane onto a support tube for permeation/reaction study is to fill the gap between the membrane and the support tube with a sealing material. In this work, the configurations to seal disk-shape dense ceramic membranes on the support tube are shown in Fig. 7, where a ceramic glass ring, a ceramic bond (P24, Tokuriki Chemical) and Ag

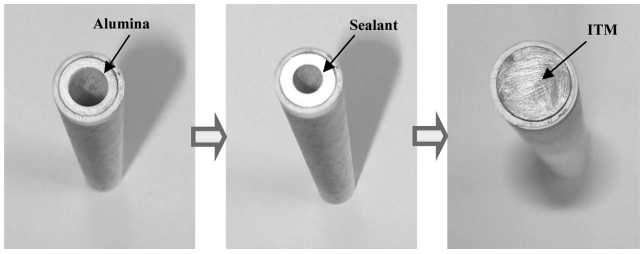

Fig. 7. The configuration to seal disk-shape dense ceramic membrane on the support tube.

ring (Ag plate, 99.9%, Aldrich) were used as the sealant to seal the disk onto the dense alumina tube.

In the case of glass ring and Ag ring, the sealing material is first melted at a higher temperature and then solidified after cooling down to the temperature range where the permeation/reaction experiments are to be performed. For a glass seal, the seal remained gas-tight in all these experiments except for one case where the temperature was too high (>950 °C), but the seal powder that filled in the gap reacted with the membrane resulting in the change of composition in the membrane. Fig. 8 shows the surface of the wetting and reacting membrane after long run test. It is known that the effective membrane surface area decreases with permeation time because of the wetting and spreading of glass to inner membrane. Consequently, the diffusion of glass seal into the membrane may cause a large portion of the membrane in contact with the seal to be ineffective, leading to large errors in flux calculation due to uncertainty in the exact permeation area for the disk-shaped membranes. Moreover, the glass type sealant reacted with the membrane to form secondary phase after long time permeation over 160 h (see spreading region in Fig. 11).

In contrast, a silver plate seal had chemical inertness and durability at high temperature. However, melted metal does not wet easily the surface of ceramics due to incompatibility in surface tension. As a result, it is difficult to obtain a perfect gas-tight seal by silver plate in comparison with glass ring. In the case of a ceramic bond, gas-tightness cannot be achieved for every test due to the difference of thermal expansion between sealant and membrane. Furthermore, the bonding of ceramic bond in the adhesive part is too strong that the membrane could not be removed easily from the support tube without physical damage to the membrane or the support.

3. Oxygen Permeation of LSCF Membrane

The oxygen permeation study was performed with CA-LSCF-6428 because CA-LSCF-6428 oxide has a single perovskite structure. After sealing with glass seal at 950 °C, oxygen in equipment was removed by introduction of N_2 gas, and then helium and air were introduced to the lines. Time dependence of oxygen permeation flux of dense CA-LSCF-6428 membrane disks is shown in Fig. 9. After the introduction of helium, one side of the membrane disc changed from high oxygen partial pressure (air side, P_{O_2}=0.21 atm) to low oxygen partial pressure (He sweep side), then an oxygen content gradient was gradually established in the membrane. The unsteady permeation flux is attributed to two aspects, as reported by Zongping Shao: One is the permeation flux due to diffusion, which increases with the increase of oxygen gradient in the membrane until a steady value is reached, and another is the time-dependent

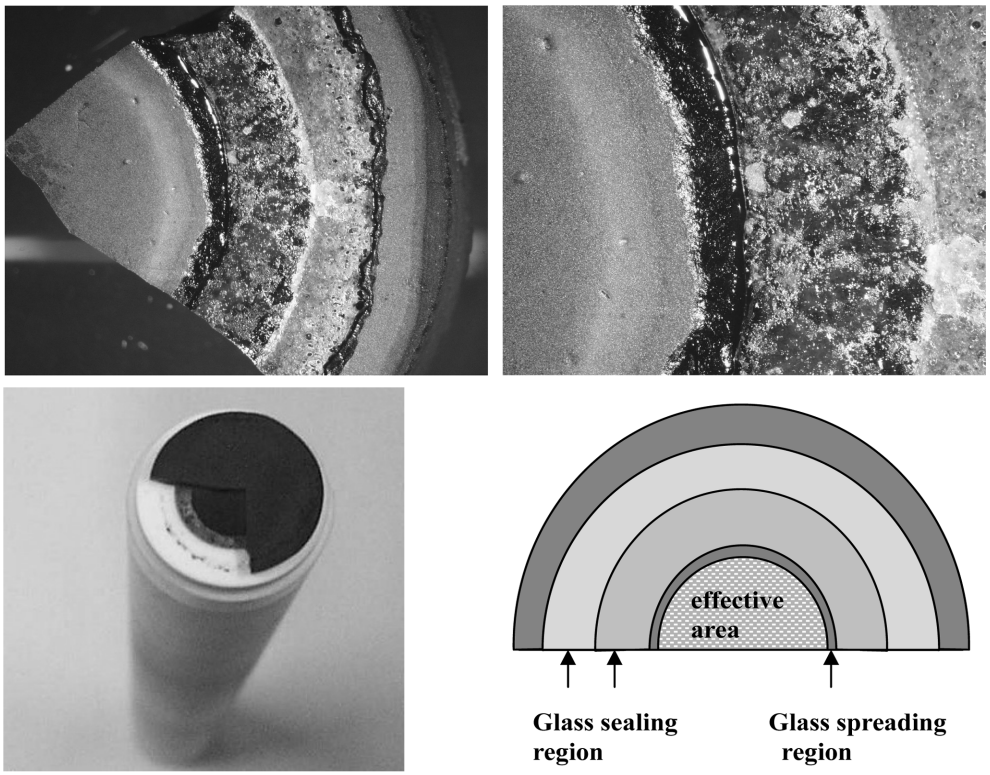

Fig. 8. The surface of the CA-LSCF-6428 membrane after permeation for 160 h.

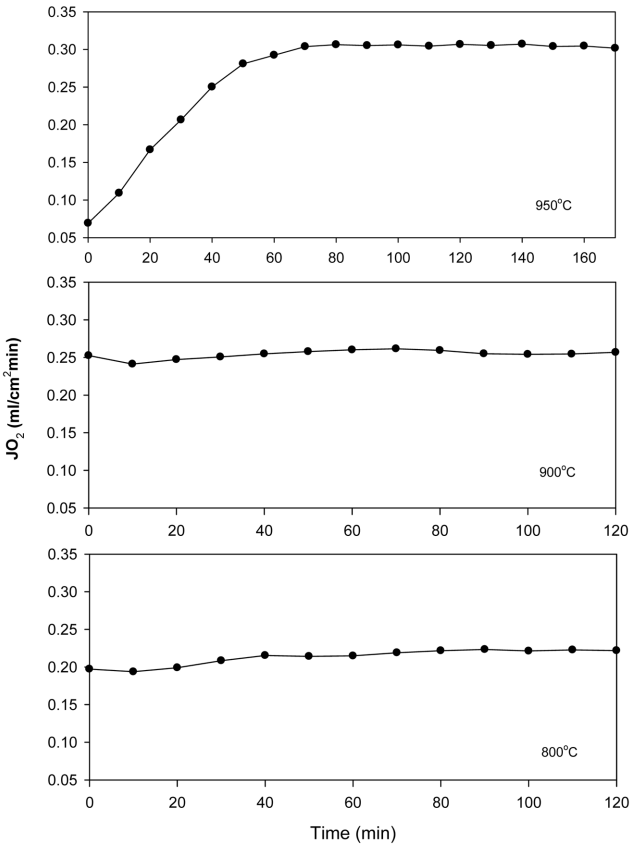

Fig. 9. Time-dependence of oxygen permeation through CA-LSCF-6428 membrane with thickness of d=1.50 mm at different temperature.

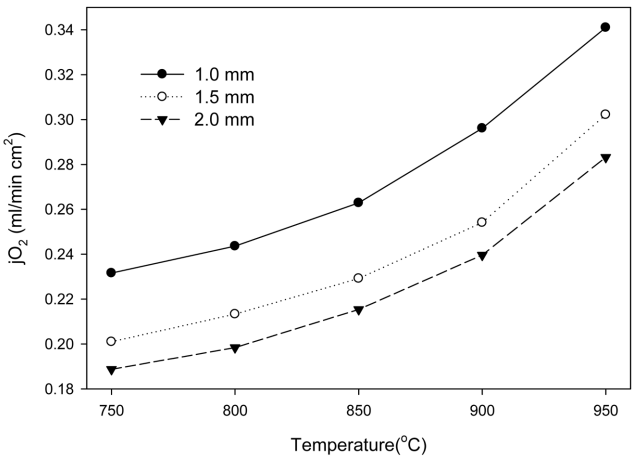

Fig. 10. Temperature-dependence of oxygen permeation through CA-LSCF-6428 membrane with different thicknesses at synthetic air/He.

contribution from the loss of lattice oxygen, which usually decreases with the elapse of time [15]. As shown Fig. 9, it was known that the time needed to reach steady state for the permeation flux was relatively short for the CA-LSCF-6428 membrane, i.e., less than 100 min for every run, irrespective of the reaction temperature. The time required to reach steady-state operation is much shorter than that (20 h) reported for LSCF by other researchers [11], while our results are in agreement with that (60 min) of the Shiguang Li et al. [16]. The reason is not immediately clear, but it may be the particular effect on the permeation equipment or the synthesized method. In the present permeation study, all data were collected after the

Table 1. Comparison of oxygen permeation properties of LSCF-6428 reported in the literatures

Studies	Temperature [°C]	Thickness [mm]	Oxygen flux [mL/min/cm^2]	Condition
Weber [18]	850	2.5	0.22	Diameter 25 mm P_{O_2} (N_2 side)=0.1 atm
Xu [11]	850	1.57	0.137	Diameter 17 mm
	963	1.65	0.31	P_{O_2} (N_2 sude)=0.002-0.004 atm
Lim [17]	850	1.7	0.17	Diameter 25 mm
	950	1.9	0.31	P_{O_2} (He side)=0.004 atm

disks had been exposed to oxygen vs. helium gradient for at least 100 min.

Oxygen permeation fluxes through dense CA-LSCF-6428 membrane disks at different temperatures and thicknesses are shown in Fig. 10. The results demonstrate that the O_2 fluxes in the measurement range of temperatures increase rapidly with the increase of the temperature and the decrease of the thickness. Table 1 shows the comparison of oxygen permeation properties of CA-LSCF-6428 reported in the literature [11,17,18]. These fluxes in Table 1 are similar to results in Fig. 10, though small differences between flux data exist. These differences may originate from the permeation equipment, operation condition and membrane characteristics. The oxygen permeation flux through 1.0 mm CA-LSCF-6428 membrane exposed to flowing synthetic air (P_h=0.21 atm) and helium (P_l=0.037 atm) reaches to a maximum, ca. 0.33 ml/cm^2·min. The increase of flux with increasing temperature is due to the increasing diffusion rate, while the effect of thickness on the increase of flux is explained by the relationship between flux and thickness, which is generally described by Wagner's Eq. (2), when the oxygen flux is governed by bulk diffusion [19].

$$J_{O_2} = \frac{RT}{16F^2L}\frac{\sigma_e\sigma_i}{(\sigma_e+\sigma_i)}\ln(P_h/P_l) \quad (2)$$

Here J_{O_2} (mol/cm^2·min) is the oxygen flux, σ_e (S/cm) is the electronic conductivity, σ_i (S/cm) is the ionic conductivity, R (J/mol·K) is the gas constant, F (C/mol) is the Faraday constant, T (K) is the temperature, L (cm) is the thickness of the membrane, P_h (Pa) is the oxygen partial pressure of the membrane surface of the high oxygen partial pressure side (air side) and P_l (Pa) is the oxygen partial pressure of the membrane surface of the lean oxygen side (reaction side or helium sweep side). The rate at which oxygen permeates through a dense membrane is essentially controlled by two factors: the rate of oxygen diffusion across the membrane, and the rate of interfacial oxygen exchange. The oxygen flux can be increased by reducing the thickness of membrane, until its thickness becomes less than a characteristic value L_c (μm) at which point the flux of oxygen is under conditions of mixed control of the surface exchange kinetics and bulk diffusion. Below L_c, the oxygen flux can only marginally be improved by making the membrane thinner [3]. Bouwmeester et al. calculated the characteristic thickness for several La-Sr-Co-Fe perovskite oxides to be in the 20 to 500 μm range at 900 °C. In this work, all membrane thickness was larger than 1.0 mm, so the oxygen flux is limited by bulk oxygen diffusion and explained through Eq. (2).

4. Membrane Stability

For industrial applications, the membrane material must exhibit long-term phase stability under the operating conditions. The oxygen permeation flux of the CA-LSCF-6428 membrane operated for 100 h in an oxygen/helium gradient at 950 °C started to decrease after several hours, and after a permeation test, the decrease of flux reached to about 9.1% (100 h) and 13.6% (160 h), in comparison with initial flux. The decrease of O_2 flux with the elapse of time may be the time-dependent contribution from the loss of lattice oxygen and structural segregation. In addition, as mentioned before, this flux decrease with permeation time can occur due to spreading of glass to inner membrane (decrease of active permeation area). To verify the crystal structure segregation, XRD analysis was conducted for both effective surfaces of the membrane after oxygen permeation. XRD analysis of the CA-LSCF-6428 membrane after permeation, as shown in Fig. 11, indicates that membrane structure is changed irrespective of the spreading of glass. XRD result in glass spreading region shows the surface of glass spreading region is an amorphous phase due to the property of glass, while the segrega-

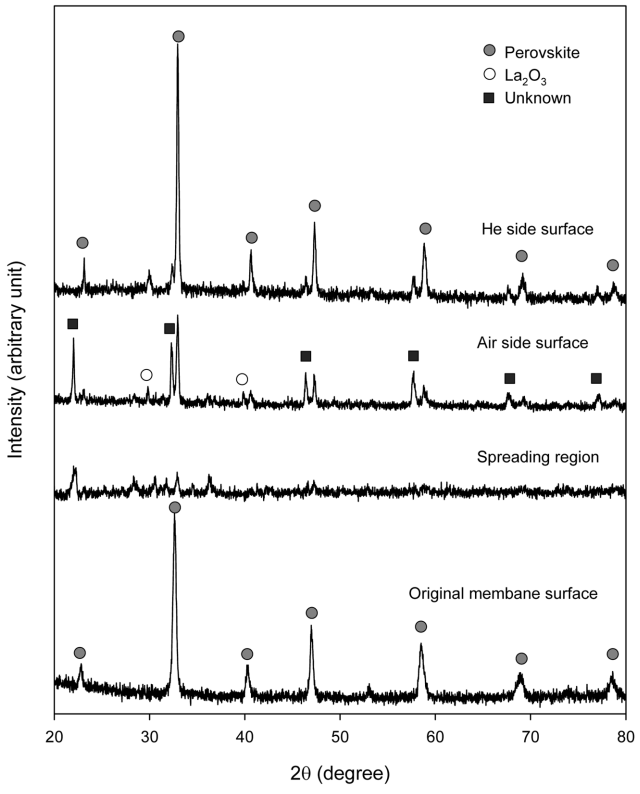

Fig. 11. The crystal structure change in the CA-LSCF-6428 membrane after oxygen permeation for 160 h.

tion is detected on the surface which is independent of glass spreading region. As shown, La_2O_3 and unknown compound are present on the membrane surface exposed to air, and a small amount of unknown compound is detected on the membrane surface exposed to helium. Li et al. [20] reported that $SrSO_4$, $CoSO_4$, SrO, Co_2O_3, and La_2O_3 were formed on the surfaces of the tubular LSCF-6428 membrane due to interaction with trace SO_2 in the air and helium, and segregation of surface elements. However, in our work, no sulfur compounds were formed both surfaces of the CA-LSCF-6428 membrane. The unknown compound could not be identified in spite of comparison with binary metal oxides (SrO, Co_2O_3, CoO, Fe_2O_3 etc.) and sulfates ($SrSO_4$, $CoSO_4$, etc.), but the result that La_2O_3 is present on the surface exposed to air indicates that segregation of surface elements occurs after long-term oxygen permeation. Though the perovskite phase is still present on the membrane surface, the XRD intensity of the perovskite must be very different from that of the original membrane surface, and the segregation occurs more excessively on the membrane surface exposed to air than on the membrane surface exposed to helium. The segregation formed on the surface may decrease either the rate of bulk diffusion or surface reaction, causing a decrease in the oxygen permeation flux.

CONCLUSIONS

Perovskite type ceramic oxides ($La_{0.6}Sr_{0.4}Co_{0.2}Fe_{0.8}O_{3-\delta}$) were synthesized by citrate method and hydrothermal method. The characterization results showed that the oxides prepared by citrate method possessed good crystal structure without secondary phase compared with the hydrothermal oxides. Contrary to crystal structure, hydrothermal method is better than citrate method for the powder morphology and particle size distribution. If single phase perovskite type oxide is obtained by hydrothermal reaction, it can be more positive over other preparation methods such as solid state reaction and citrate method.

Good wettability, thermal expansion coefficient, chemical inertness and adequate bonding strength were investigated for inorganic sealing materials for dense ionic-conducting ceramic membranes. Pyrex glass seal and Ag melting seal provided reliable gas-tight sealing of disk type dense membrane at high temperature, but in the case of commercial ceramic binder, gas-tightness could not be achieved for every test due to the difference of thermal expansion between sealant and membrane. Though the degree of gas tightness increases in the order of glass>Ag>ceramic binder, the undesired spreading of glass leads to an interfacial reaction between it and the perovskite membrane. Therefore, sealing by exerting a compression force on the metal ring is the best option for long time operation.

The oxygen flux of $La_{0.6}Sr_{0.4}Co_{0.2}Fe_{0.8}O_{3-\delta}$ membrane increased with increasing temperature and decreasing thickness, and the oxygen permeation flux through 1.0 mm membrane exposed to flowing air (P_h=0.21 atm) and helium (P_l=0.037 atm) was ca. 0.33 ml/cm^2·min at 950 °C. Continuous operation of the perovskite membrane led to decrease of oxygen permeation due to segregation of the surface elements as well as the spreading of glass sealing material into inner membrane. XRD analysis after 160 h continuous operation indicated that La_2O_3 and unknown compound were formed on the surface of membrane regardless of the interfacial reaction between glass and membrane.

ACKNOWLEDGMENT

This Research was supported by a grant (AC2-101) from Carbon Dioxide Reduction Sequestration Research Center, one of the 21st Century Frontier Programs funded by the Ministry of Science and Technology of Korean government.

NOMENCLATURE

$F_{permeation}$: permeation flux [ml/min]
y_{O_2} : oxygen concentration [v%]
A : effective membrane surface area [cm^2]
P_{O_2} : oxygen partial pressure [Pa]
d : membrane thickness [mm]
J_{O_2} : oxygen flux [mol/cm^2·min]
R : gas constant [J/mol·K]
T : temperature [K]
F : Faraday constant [C/mol]
L : thickness of the membrane [cm]
P_h : oxygen partial pressure at oxygen-rich side [Pa]
P_l : oxygen partial pressure at oxygen-lean side [Pa]

Greek Letters

σ_e : electronic conductivity [S/cm]
σ_i : ionic viscosity [S/cm]
θ : angle [radian]

REFERENCES

1. D. Gielen and J. Podkanski, *Prospects for CO_2 capture and storage*, IEA Publictions, Paris (2004).
2. K. Thambimuthu, M. Soltanieh and J. C. Abanades, in *IPCC special report on carbon dioxide caopture and storage*, O. Davidson and B. Metz Eds., Cambridge University Press, London (2005).
3. A. J. Burggraaf and H. J. M. Bouwmeester, in *Fundamentals of inorganic membrane science and technology*, A. J. Burggraaf and L. Cot Eds., Elsevier, Amsterdam (1996).
4. P. N. Dyer, R. E. Richards, S. L. Russek and D. M. Taylor, *Solid State Ion*, **134**, 21 (2000).
5. Y. Teraoka, H. M. Zhang, S. Furukawa and N. Yamazoe, *Chem. Lett.*, 1743 (1985).
6. Y. Teraoka, T. Nobunaga and N. Yamazoe, *Chem. Lett.*, 503 (1988).
7. Y. Teraoka, T. Nobunaga, K. Okamoto, N. Miura and N. Yamazoe, *Solid State Ion*, **48**, 207 (1991).
8. S. Carter, A. Selcuk, R. J. Chater, J. Kajda, J. A. Kilner and B. C. H. Steele, *Solid State Ion.*, **53**, 597 (1992).
9. Y. Zeng, Y. S. Lin and S. L. Swartz, *J. Membr. Sci.*, **87**, 150 (1998).
10. S. J. Xu and W. J. Thomson, *AIChE J.*, **43**, 2731 (1997).
11. S. J. Xu and W. J. Thomson, *Ind. Eng. Chem. Res.*, **37**, 1290 (1998).
12. J. A. Lane, S. J. Benson, D. Waller and J. A. Kilner, *Solid State Ion*, **121**, 201 (1999).
13. Q. Xu, D. Huang, W. Chen, J. H. Lee, H. Wang and R. Yuan, *Scripta Materialia*, **50**, 165 (2004).
14. W. Jin, S. Li, P. Huang, N. Xu and J. Shi, *J. Membr. Sci.*, **170**, 9 (2000).
15. Z. Shao, W. Yang, Y. Cong, H. Dong, J. Tong and G. Xiong, *J. Membr. Sci.*, **172**, 177 (2000).

16. S. Li, W. Jin, P. Huang, N. Xu and J. Shi, *AIChE J.*, **45**, 276 (1999).
17. K. S. Lim, K. S. Lee, I. S. Han, D. W. Seo, K. S. Hong, K. Bai, S. K. Woo and T. L. Cho, *Journal of the Korean Ceramic Society*, **38**, 886 (2001).
18. W. J. Weber, J. W. Stevenson, T. R. Armstrong and L. R. Pederson, in *Mater*. Res. Soc. Symp. Proc., G. A. Nazri, J. M. Taracson and M. S. Scheiber Eds., Materials Research Society, Pittsburgh (1995).
19. N. Itoh, T. Kato, K. Uchida and K. Haraya, *J. Membr. Sci*., **92**, 239 (1994).
20. S. Li, W. Jin, P. Huang, N. Xu, J. Shi and Y. S. Lin, *J. Membr. Sci*., **166**, 51 (2000).